MOLECULAR AND CELLULAR BIOLOGY, June 2002, p. 3864–3874 Vol. 22, No. 11
0270-7306/02/$04.00+0 DOI: 10.1128/MCB.22.11.3864–3874.2002

The PERK Eukaryotic Initiation Factor 2α Kinase Is Required for the Development of the Skeletal System, Postnatal Growth, and the Function and Viability of the Pancreas

Peichuan Zhang,[1] Barbara McGrath,[1] Sheng'ai Li,[1] Ami Frank,[1] Frank Zambito,[1] Jamie Reinert,[1] Maureen Gannon,[2] Kun Ma,[3] Kelly McNaughton,[4] and Douglas R. Cavener[1,4]*

Department of Biology, The Pennsylvania State University, University Park, Pennsylvania 16802[1]; Departments of Medicine and Molecular Physiology and Biophysics, Vanderbilt University School of Medicine,[2] and Department of Molecular Biology, Vanderbilt University,[4] Nashville, Tennessee 37235; and Department of Biochemistry and Molecular Biology, Indiana University School of Medicine, Indianapolis, Indiana 46202[3]

Received 12 December 2001/Returned for modification 6 February 2002/Accepted 21 February 2002

Phosphorylation of eukaryotic initiation factor 2α (eIF-2α) is typically associated with stress responses and causes a reduction in protein synthesis. However, we found high phosphorylated eIF-2α (eIF-2α[P]) levels in nonstressed pancreata of mice. Administration of glucose stimulated a rapid dephosphorylation of eIF-2α. Among the four eIF-2α kinases present in mammals, PERK is most highly expressed in the pancreas, suggesting that it may be responsible for the high eIF-2α[P] levels found therein. We describe a *Perk* knockout mutation in mice. Pancreata of $Perk^{-/-}$ mice are morphologically and functionally normal at birth, but the islets of Langerhans progressively degenerate, resulting in loss of insulin-secreting beta cells and development of diabetes mellitus, followed later by loss of glucagon-secreting alpha cells. The exocrine pancreas exhibits a reduction in the synthesis of several major digestive enzymes and succumbs to massive apoptosis after the fourth postnatal week. $Perk^{-/-}$ mice also exhibit skeletal dysplasias at birth and postnatal growth retardation. Skeletal defects include deficient mineralization, osteoporosis, and abnormal compact bone development. The skeletal and pancreatic defects are associated with defects in the rough endoplasmic reticulum of the major secretory cells that comprise the skeletal system and pancreas. The skeletal, pancreatic, and growth defects are similar to those seen in human Wolcott-Rallison syndrome.

Protein synthesis in secretory cells is episodically regulated to meet the rapidly changing demands for secreted proteins that participate in physiological and developmental processes. A prime example of episodic regulation of protein synthesis is the endocrine and exocrine pancreas, which responds within minutes of nutritional stimulation to secrete a panoply of stored peptide hormones and digestive enzymes. In the wake of secretion, synthesis of secretory proteins is activated to replenish the pools of stored proteins released from secretory granules (11, 19, 24, 27, 40). As secretion subsides and the newly synthesized secretory proteins reach a critical concentration in the secretory granules, Golgi, and rough endoplasmic reticulum (RER), the synthesis of these proteins is repressed.

In the endocrine pancreas, the regulation of insulin secretion by the beta cells of the islets of Langerhans continues to be one of the most intensely investigated regulatory processes (30). The ingestion of glucose stimulates insulin secretion within a few minutes and results in rapid insulin-induced glucose import into most cells of the body. Following induction of insulin secretion, both global protein synthesis and preproinsulin synthesis are derepressed from the relatively low levels observed in the fasted state. The regulation of protein synthesis and preproinsulin synthesis is poorly understood. Translational control exerted through the regulation of mRNA cap binding proteins and the regulation of the eukaryotic initiation factor 2 (eIF-2)–GTP–Met-tRNAi ternary complex have been implicated in the regulation of protein synthesis in the insulin-secreting beta cells, but definitive biochemical and genetic analysis is lacking. The exocrine pancreas is stimulated to secrete a complex of diverse digestive enzymes by a variety of stimuli, including acetylcholine, gastrin, and cholecystokinin (30). Despite the fact that cotranslational import of proteins into the ER was first discovered and extensively characterized in the pancreatic acinar cells (10, 25, 38), the fundamental mechanisms underlying the highly dynamic regulation of protein synthesis in the exocrine pancreas have not been elucidated.

Similar to pancreatic cells in their extraordinary secretory capacity are chondrocytes and osteoblasts, the major secretory cells of the skeletal system, which are responsible for the massive secretion of the cartilage and bone matrix proteins that occurs during prenatal and postnatal development. The synthesis and secretion of collagen and other extracellular proteins that comprise cartilage and bone matrix are dynamically regulated as a consequence of the complexity of the growth of the skeletal system, as well as changes in serum levels of growth factors, calcium, and nutrients.

Clues to the regulation of protein synthesis in secretory cells have recently come from the investigation of the unfolded protein response (UPR) (3, 13, 20), an adaptive mechanism to thwart the deleterious effects of accumulating toxic concentrations of unfolded proteins in the ER. The UPR in higher

* Corresponding author. Mailing address: Department of Biology, 208 Mueller Lab, The Pennsylvania State University, University Park, PA 16802. Phone: (814) 865-4562. Fax: (814) 865-6193. E-mail: drc9@psu.edu.

eukaryotes involves transcriptional activation of the folding and chaperone proteins along with repression of global protein synthesis. Recently, an eIF-2α kinase, denoted PERK/PEK, has been discovered and is responsible for UPR-induced repression of protein synthesis (14, 32).

PERK is hyperactivated by pharmacological agents that disturb the Ca^{2+} balance, protein folding, or glycosylation in the ER (13). Phosphorylation of eIF-2α by PERK under these extreme conditions results in global repression of protein synthesis. Among the eIF-2α kinase family, PERK is uniquely present in the ER as a type 1 transmembrane protein, and its activity is regulated by the BiP/GRP78 ER resident protein chaperone (3, 13). Through the interaction of BiP/GRP78 with the ER lumenal domains of PERK and IRE1, it has been proposed that BiP/GRP78 negatively regulates PERK and IRE1 by blocking their ability to form oligomers or homodimers. When the folding capacity of the ER is exceeded, either by increasing the concentration of unfolded proteins or by decreasing the folding or chaperone proteins, BiP/GRP78 disassociates from PERK, allowing it to form activated homomeric complexes. Hyperactivated PERK results in the repression of global protein synthesis and may further result in apoptosis. Based upon these findings, PERK has been categorized as a stress-related protein. However, we have discovered that PERK is abundantly expressed in secretory and endocrine organs, including the exocrine and endocrine pancreas, as well as osteoblasts, which secrete type I collagen, the most abundant protein in the body. Although PERK is thought to be expressed at low levels in virtually all cells, the high level of expression in secretory cells suggested to us that PERK may have an important regulatory role in secretory cells under normal physiological conditions.

In addition to PERK, mammalian species contain three other eIF-2α kinases: GCN2, HRI, and PKR (2, 5, 15, 33, 34, 39). Each of the eIF-2α kinases is activated by different factors, but all specifically phosphorylate Ser51 of eIF-2α. Phosphorylated Ser51 eIF-2α, complexed with eIF-2β, eIF-2γ, and GDP, blocks the GDP-GTP exchange reaction by sequestering the eIF-2B guanylate exchange factor in an inactive state. In the absence of eIF-2B activity, the eIF-2–GTP–Met-tRNAi ternary complex cannot be replenished for subsequent rounds of translation initiation (6). In the extreme, hyperphosphorylation of eIF-2α results in complete repression of global protein synthesis followed by cell death. However, more moderate levels of phosphorylated eIF-2α (eIF-2α[P]) can actually stimulate the translation initiation of specific mRNAs encoding regulatory proteins, as has been elegantly demonstrated for the yeast GCN4 transcriptional activator of amino acid biosynthesis (16–18).

Mammalian cells typically contain a low level of eIF-2α[P]; however, we show herein that eIF-2α is highly phosphorylated in the pancreas by PERK during the fasted state. Upon glucose stimulation, eIF-2α is dephosphorylated over the same time course as the induction of insulin synthesis. These data further suggest that PERK may play an important role in regulating protein synthesis in secretory cells. To determine the role of PERK in regulating protein synthesis in secretory organs and tissues, we generated a knockout mutation of the mouse *Perk* gene. We show that a fraction of homozygous *Perk* mutants are viable but display a number of severe defects in pancreatic functions, are growth retarded, and exhibit multiple skeletal dysplasias. These defects are associated with major shifts in the synthesis of secretory proteins, misregulation of genes that function in protein secretion, gross abnormalities in the RER, and apoptotic cell death.

MATERIALS AND METHODS

Cloning and targeted disruption of the *Perk* gene. A 14.0-kb region of the *Perk* gene was isolated from a lambda genomic library of a 129 SvEvTac mouse strain. Exon sequences were determined by comparison of a PERK cDNA clone with the genomic DNA sequence. To generate a targeted deletion of essential domains of the *Perk* gene, loxP sites were inserted into intronic sequences flanking three exons that encode part of the lumenal domain, the transmembrane domain, and part of the catalytic domain. The floxed *Perk* gene fragment and flanking genomic sequences were cloned into the phosphoglycerol kinase-neomycin loxP (pGK-neo loxP) targeting vector. The PERK-neo-lox targeting vector was electroporated into Tl1 129 SvEvTac mouse embryonic stem cells. Eight of 396 neomycin-resistant clones (2.0%) were characterized as homologous recombinants by Southern blotting and PCR analyses. Homologous recombinant cells were transplanted into C57BL/6 blastocysts. Four chimeric founder mice were shown to have the PERK-lox-neo gene in their germ lines (data not shown). The PERK-lox-neo mice were mated to transgenic mice expressing Cre recombinase under the control of the EIIa promoter (DuPont Pharmaceutical Company and the Jackson Laboratory). Cre-mediated deletion of the region between loxP sites was detected by PCR and confirmed by sequence analysis.

Immunoblot analysis of pancreatic tissue. Prediabetic (11 to 12 days old) and diabetic (26 to 28 days old) $Perk^{-/-}$ mice and wild-type littermates were euthanized by CO_2 asphyxiation. The entire pancreas was placed in 300 μl of homogenization buffer (9 M urea, 0.02% Triton X-100, 0.1 M dithiothreitol [DTT], 1× protease inhibitor cocktail for tissues and cells σ, 1× phosphatase inhibitor cocktail I σ) and sonicated on ice. Samples were incubated on ice for 5 to 10 min prior to centrifugation at 10,000 × *g* for 10 min at 4°C. The supernatants were transferred to fresh tubes and kept on ice. Total protein was determined using the Bio-Rad protein assay (Bio-Rad).

Samples were electrophoresed on 4-to-15% gradient polyacrylamide–sodium dodecyl sulfate gels (Bio-Rad) and then transferred to Hybond ECL membranes (Amersham/Pharmacia) by using the Bio-Rad Transblot semidry transfer system. Membranes were blocked for 1 h at room temperature in Chemicon blocking solution (Chemicon) diluted 1:4 in Tris-buffered saline plus 0.1% Tween 20 (TBST). Incubation in primary antibodies was carried out for 1 h at room temperature or overnight at 4°C. Antibodies were diluted into Chemicon blocking solution at the following dilutions: anti-mouse eIF-2α, 1:1,000; anti-mouse eIF-2α[P] (Biosource International), 1:750; rabbit anti-human PERK (anti-hPEK; Ron Wek, Indiana University School of Medicine), 1:1,000; anti-human BiP (Santa Cruz), 1:200; anti-human Hsc70 (Santa Cruz), 1:200; anti-mouse ERp72 (Stressgen), 1:1,000; anti-human pancreatic α-amylase (Biodesign), 1:5,000; anti-human lipase (Biodesign), 1:5,000; anti-bovine pancreatic carboxypeptidase A (Rockland), 1:5,000; anti-porcine pancreatic carboxypeptidase B (Rockland), 1:5,000; anti-bovine pancreatic DNase (Rockland), 1:2,000; anti-bovine pancreatic RNase (Rockland), 1:2,000; anti-bovine pancreatic trypsinogen (Rockland), 1:5,000; and anti-α-tubulin (Sigma), 1:1,000. The ability of the non-mouse antibodies to detect mouse proteins reflects their considerable homology across species. After incubation with primary antibodies, the membranes were washed three times for 10 min in TBST. Horseradish peroxidase-conjugated secondary antibodies (Jackson ImmunoResearch) were diluted 1:5,000 in Chemicon blocking solution and incubated with the blots for 1 h at room temperature with gentle agitation. Membranes were washed three times for 10 min in TBST. Immunoreactive bands were visualized by chemiluminescent detection with the ECL Plus kit (Amersham/Pharmacia) on a Storm 860 Phosphorimager (Molecular Dynamics/Amersham/Pharmacia). Band intensities were measured using ImageQuant (Molecular Dynamics/Amersham/Pharmacia). Intensity values were normalized to the housekeeping proteins α-tubulin or actin.

Determination of blood glucose and serum insulin. For routine blood glucose measurements in nonterminal procedures, blood samples were obtained from the tail. Blood was also taken from the saphenous vein in nonterminal procedures to provide sufficient amounts to test both blood glucose and insulin levels. In terminal procedures, cardiac blood was used for both glucose and circulating insulin measurements. Blood glucose was measured with the AccuChek glucose monitor. Serum for insulin analysis was collected from the saphenous vein or cardiac blood and separated using Microvette CB300 serum separators (Sarstedt) following the manufacturer's instructions. Serum insulin was mea-

sured by enzyme-linked immunosorbent assay (ELISA; Crystal Chem). *Perk*$^{-/-}$ mice and wild-type littermates (7 to 11 days old and 30 to 43 days old) were euthanized by CO_2 asphyxiation. The pancreata were removed and their wet weights were determined. Pancreata were subjected to acid-ethanol extraction (28) with the following modifications: pancreas tissue was briefly homogenized on ice in ice-cold acid-ethanol (1.5% HCl in 75% ethanol; 20 μl/mg [wet weight]). Homogenates were rocked overnight at 4°C. Insoluble material was removed by centrifugation at 20,000 × *g* for 1 h at 4°C. Extracts were neutralized to pH 7.0 with 1 M Tris base. Insulin concentrations were determined by ELISA (Crystal Chem).

Immunohistochemistry. Pancreata were isolated from *Perk*$^{+/+}$ and *Perk*$^{-/-}$ mice, fixed in 4% paraformaldehyde–0.1 M phosphate buffer, dehydrated, and paraffin-embedded for serial sectioning (5 μm thick). Rabbit anti-mouse insulin (1:1,000), rabbit antiglucagon (1:250; Santa Cruz), and rabbit anti-mouse eIF-2α[P] (1:250; Research Genetics) were used as primary antibodies for immunohistochemical analyses. Fluorescent double-labeling experiments were carried out using rabbit antiglucagon and guinea pig anti-bovine insulin primary antibodies (Linco Research) and Cy2-conjugated donkey anti-guinea pig immunoglobulin G (IgG; 1:500) and Cy3-conjugated donkey anti-rabbit IgG (1:500) secondary antibodies (Jackson ImmunoResearch). Apoptosis analysis was performed using the Apoptosis Detection System (Promega) according to the manufacturer's protocol.

Analysis of the skeletal system. Mouse skeletons were fixed in 10% neutral buffered formalin, rinsed with double-distilled H_2O, and postfixed in 70% ethanol. Cartilage tissues of the specimens were stained with 0.2% Alcian Blue 8GX (Sigma) in ethanol-glacial acetic acid and treated with 1.0% trypsin in 30% saturated sodium borate. Mineralized bone was stained with Alizarin Red (Sigma) in 0.5% KOH, treated with a graded series of KOH-glycerol, and stored in glycerol with a crystal of thymol.

Isolation of calvaria and culture of primary osteoblasts. Osteoblasts were isolated from intact bone and cultured as described by Ecarot-Charrier et al. (9). Briefly, calvaria (frontal and parietal bones) from 10-day-old mice were removed and the periosteal layers on both sides and any remaining meninges were carefully stripped off with forceps in Dulbecco's modified Eagle's medium buffered with 15 mM HEPES, pH 7.4 (DMEM; Gibco). Each calvaria was transferred to a 35- by 10-mm cell culture dish containing 2 ml of DMEM supplemented with 10% fetal calf serum and 1% penicillin-streptomycin. Glass shards obtained from crushed coverslips (Corning) were spread over the entire endocranial surface and then cleared away from sutures. After 6 days in culture, cells adhered to the glass shards were flushed and scraped off the cranial surface and grown in the culture medium for 2 to 3 weeks until they reached confluence. The medium was changed every 3 days.

Immunoblot analysis of bone tissues and primary osteoblasts. For bone tissues, mouse long bones (tibia, femur, and humerus) and vertebrae were isolated, with the bone marrow being carefully removed. The bone tissue was minced with a scalpel and scissors and rapidly transferred to the homogenization buffer, which contained 9 M urea, 0.02% Triton X-100, 0.1 M DTT, 5% trichloroacetic acid, 1× protease inhibitor cocktail for tissues and cells (Sigma), 1× phosphatase inhibitor cocktail I (Sigma), and 2 mM *N*-ethylmaleimide. The bone tissue was homogenized on ice with a Polytron homogenizer. The bone samples were decalcified by incubation in lysis buffer at 4°C for 2 days. The bone tissue was then processed for immunoblot analysis as described above.

For primary osteoblasts, the cells were cultured as described above for 2 to 3 weeks until they reached confluence. The osteoblasts were then solubilized in lysis buffer containing 9 M urea, 0.02% Triton X-100, 0.1 M DTT, 1× protease inhibitor cocktail for tissues and cells (Sigma), and 1× phosphatase inhibitor cocktail I (Sigma). The samples were then processed for immunoblot analysis as described above.

Antibodies for both bone tissue and osteoblasts were diluted into Chemicon blocking solution at the following dilutions: anti-goat procollagen I α2 (Santa Cruz), 1:200; anti-rabbit collagen I (Rockland), 1:500; anti-rabbit actin (Sigma), 1:1,000; and anti-α-tubulin (Sigma), 1:1,000. Horseradish peroxidase-conjugated secondary antibodies (Jackson ImmunoResearch) were diluted 1:5,000 in Chemicon blocking solution and processed as described above.

TEM. Bone and pancreas tissues were isolated and initially fixed in 2.5% glutaraldehyde, 4% paraformaldehyde in 0.1 M sodium cacodylate buffer. Secondary fixation was with 1% osmium tetroxide in 0.1 M sodium cacodylate buffer. Samples were then stained with 2% uranyl acetate and dehydrated through an ethanol and acetone series. The samples were infiltrated and embedded in Spurr's resin over several days and polymerized at 60°C. Transmission electron microscopy (TEM) samples were sectioned using a diamond knife (70 nm thick) and stained with uranyl acetate and lead citrate. Images were captured on a JEOL 1200 EXII TEM microscope.

RESULTS

eIF-2α is highly phosphorylated in the pancreas and is dephosphorylated upon glucose stimulation. Phosphorylation of the translation initiation factor eIF-2α has been reported to be associated with a variety of stress responses in cultured mammalian cells and acts to repress global protein synthesis (13). We have examined the phosphorylation state of eIF-2α in normal mouse tissue and found that eIF-2α[P] levels are low in most tissues, as expected, but the pancreas shows exceptionally high levels (Fig. 1A). The high level of eIF-2α[P] in the pancreas was seen in the glucagon-secreting alpha cells and the insulin-secreting beta cells of the islets of Langerhans, as well as in a subpopulation of the acinar cells of the exocrine pancreas (Fig. 1B and C). The eIF-2α[P] levels were particularly high in mice that were fasted for approximately 16 h, during which time protein synthesis in the pancreas is relatively quiescent (Fig. 1D, lanes 1, 3, and 5). It is well known that the administration of glucose stimulates the pancreas to rapidly secrete insulin and other secretory proteins (11, 24, 26, 40). Protein synthesis in the pancreas is mobilized in the wake of nutritional stimulation to replenish the stores of secretory proteins. We postulated that eIF-2α[P] would be dephosphorylated prior to the derepression of protein synthesis that occurs upon glucose stimulation of the pancreas. To test this hypothesis, we examined the change in pancreatic eIF-2α[P] after the administration of glucose to previously fasted wild-type mice. We observed a fivefold reduction of eIF-2α[P], which immediately followed the rise of serum glucose and insulin (Fig. 1D and E) and is coincident with the derepression of protein synthesis (11). Within a few hours, serum glucose decreased and eIF-2α[P] increased to fasted basal levels (Fig. 1E).

PERK is highly expressed in the endocrine and exocrine pancreas. Among the four known eIF-2α kinases, only PERK mRNA has been shown to be highly expressed in the pancreas and therefore is the kinase likely responsible for the high level of eIF-2α[P] in this organ. We show herein that the PERK protein is indeed highly expressed in the pancreas, especially compared to organs that contain a small fraction of secretory cells (Fig. 1F).

Generation of *Perk* knockout mutant mice. The *Perk* gene was isolated from a mouse genomic library, and exons encoding essential domains of PERK were identified by sequence comparisons of cDNA and genomic DNA. Two synthetic loxP sites were inserted into the mouse *Perk* gene flanking exons encoding part of the ER lumenal activation domain, the transmembrane domain, and part of the cytoplasmic catalytic domain (Fig. 2A). In addition, the neomycin resistance gene (Neo^r) and a third loxP site were inserted into an intron downstream of the two loxP sites flanking critical coding exons. Mouse strains bearing the three loxP insertions and Neo^r (*Perk* loxP) were mated to a transgenic mouse strain expressing the Cre recombinase under the control of the EIIa promoter (23). The F_1 mice were screened by PCR amplification of genomic DNA for Cre-mediated recombination leading to the deletion of a segment of the *Perk* gene (as described above) and the Neo^r selectable marker (i.e., ΔloxP1–3, denoted *Perk*$^-$ heretofore). F_1 heterozygous *Perk*$^{+/-}$ mice bearing a putative germ line *Perk* deletion were crossed inter se to generate homozygous loss-of-function mutants. Several *Perk*$^{-/-}$ deletion strains

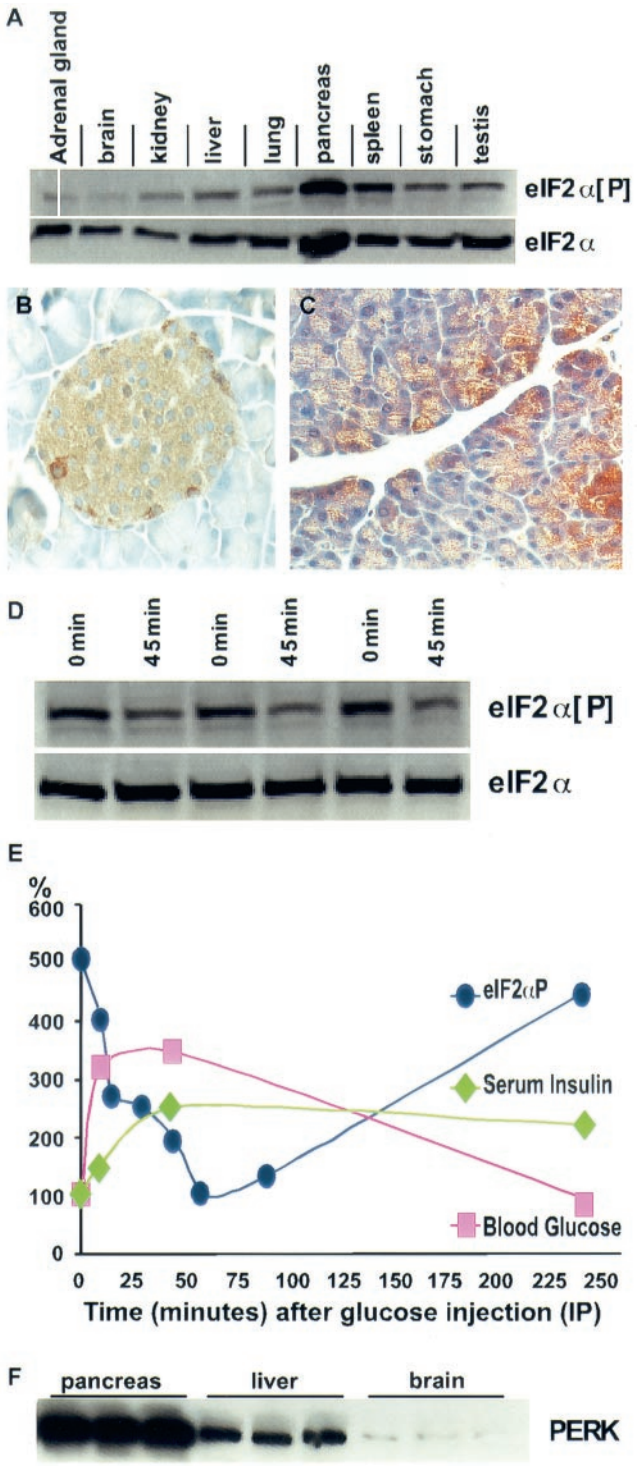

FIG. 1. Physiological regulation of eIF-2α[P] and correlated expression of PERK in the pancreas. (A) Immunoblot analysis of eIF-2α[P] shows moderate levels of expression in the spleen and high levels in the pancreas of wild-type C57BL6 mice, while most tissues exhibit a low level of eIF-2α[P]. Although the pancreas also exhibits a relatively high level of total eIF-2α (phosphorylated and nonphosphorylated), quantitative analysis indicates that the pancreas shows approximately twice the amount of eIF-2α[P] compared to other tissues after normalizing to total eIF-2α. (B and C) Cellular localization of eIF-2α[P] in the islets of Langerhans and acinar cells of wild-type mouse pancreas. (D) Pancreatic eIF-2α[P] and total eIF-2α (nonphosphorylated and phosphorylated) in pancreata from fasted mice (0 min) versus mice 45 min after the intraperitoneal injection of glucose (45 min). (E) Blood glucose (■), serum insulin (♦), and eIF-2α[P] (●) of fasted mice injected at time zero with glucose. Insulin and glucose values are normalized to time zero, and eIF-2α[P] values are normalized to total eIF-2α and to the 1-h time point. Each data point represents the average of three to five individual mice. Representative data for the fasted and glucose-injected mice are shown in panel D. Four other similar experiments were conducted over a 2-year period and resulted in a similar pattern of glucose-stimulated dephosphorylation of eIF-2α. (F) Immunoblot analysis of wild-type mice shows high levels of PERK in the pancreas, moderate levels in the liver, and low levels in the brain. C57BL/6 (Jackson Lab) male mice, 6 to 10 weeks old, were used for all glucose injection experiments described above.

were isolated and shown to lack PERK mRNA encoding the deleted domains (Fig. 2B) and they did not express PERK protein in the pancreas (Fig. 2C).

Matings between heterozygous $Perk^{+/-}$ mice do not result in the expected frequency of viable $Perk^{-/-}$ mutants; only 37% of the expected number survived beyond the first few days and at least 23% died within the first 48 h. Approximately 30 to 40% of the $Perk^{-/-}$ mice died prenatally. The surviving newborn $Perk^{-/-}$ mice were of normal size but exhibited severe postnatal growth retardation (Fig. 3A and B). At the end of the first week, the $Perk^{-/-}$ mice were typically 40 to 50% smaller than their wild-type littermates, and this growth discrepancy continued through the fourth postnatal week. As expected, the level of eIF-2α[P] was reduced ninefold in the pancreata of $Perk^{-/-}$ mice that were 7 to 12 days old (Fig. 2D), indicating that the exceptionally high level of eIF-2α[P] seen in a normal mouse pancreas is largely due to the activity of PERK.

Perk knockout mutants progressively lose pancreatic insulin-secreting beta cells and glucagon-secreting alpha cells and develop diabetes mellitus. Although insulin and blood glucose levels were nearly normal during the first three postnatal weeks, $Perk^{-/-}$ mice rapidly developed severe hyperglycemia around day 22 (Fig. 3C). Glucose tolerance tests indicated that the diabetic $Perk^{-/-}$ mice were incapable of rapidly clearing blood glucose. As a consequence of the diabetes, liver glycogen content escalated in $Perk^{-/-}$ mice to more than threefold higher than that of their wild-type littermates. The pancreata of 1-week-old $Perk^{-/-}$ mice appeared to be normal, and the distribution and number of insulin-secreting beta cells and glucagon-secreting alpha cells was normal. Beginning by the second postnatal week, the beta cells in the $Perk^{-/-}$ mice began to degenerate, while the alpha cells became dispersed throughout the islets (Fig. 4A to G). Terminal deoxynucleotidyltransferase-mediated dUTP-biotin nick end labeling (TUNEL) analysis of histological preparations of pancreatic tissues revealed that the loss of the beta cells is associated with a dramatic increase in apoptosis in $Perk^{-/-}$ mice (Fig. 4H and I). After the fourth postnatal week, very few insulin-secreting beta cells could be detected, and a rapid reduction in the number of glucagon-secreting alpha cells was seen. In some $Perk^{-/-}$ mice neither islet alpha nor beta cells could be detected after the sixth postnatal week; such mice were sacrificed due to poor health.

Total insulin content in the pancreatic islets was reduced by 32% in 17-day-old $Perk^{-/-}$ mice. However, quantitative mor-

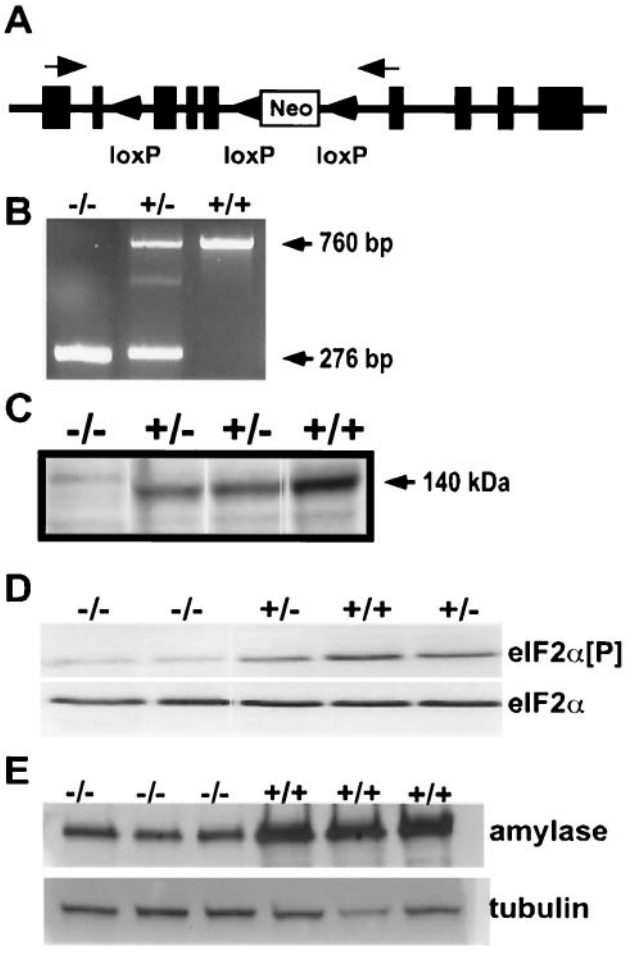

FIG. 2. Generation of *Perk*$^{-/-}$ knockout mice. (A) Schematic of targeting construct designed for generation of *Perk*$^{-/-}$ mice. Tandemly oriented loxP sites were inserted into a 14.0-kb genomic clone of the *Perk* gene and then cloned into the pGK-neo-loxP targeting vector. Black boxes represent PERK-encoding exons, and arrows indicate priming sites for RT-PCR. *Perk*$^{-/-}$ mice described in the text have suffered a deletion of all genomic DNA between the first and third loxP sites. (B) RT-PCR analysis of total RNA using primers flanking the Cre-excised exons. Both *Perk*$^{+/-}$ and *Perk*$^{-/-}$ mice produced the expected 276-bp truncated mRNA band, while both the *Perk*$^{+/-}$ and *Perk*$^{+/+}$ mice produced the expected 760-bp band, which was confirmed by sequence analysis. (C) Immunoblot of PERK from pancreatic lysates isolated from *Perk*$^{+/+}$, *Perk*$^{+/-}$, and *Perk*$^{-/-}$ mice with antisera recognizing the kinase domain of PERK. PERK is not expressed in the pancreas of *Perk*$^{-/-}$ mice, and expression is reduced in the *Perk*$^{+/-}$ mice. (D) Immunoblot analysis of eIF-2α[P] and eIF-2α from pancreatic lysates isolated from 12-day-old *Perk*$^{+/+}$, *Perk*$^{+/-}$, and *Perk*$^{-/-}$ mice. Note the greatly reduced levels of eIF-2α[P] in the *Perk*$^{-/-}$ mice. (E) Immunoblot analysis of amylase from pancreatic lysates isolated from 26- to 28-day-old *Perk*$^{+/+}$ and *Perk*$^{-/-}$ mice, using antisera for amylase.

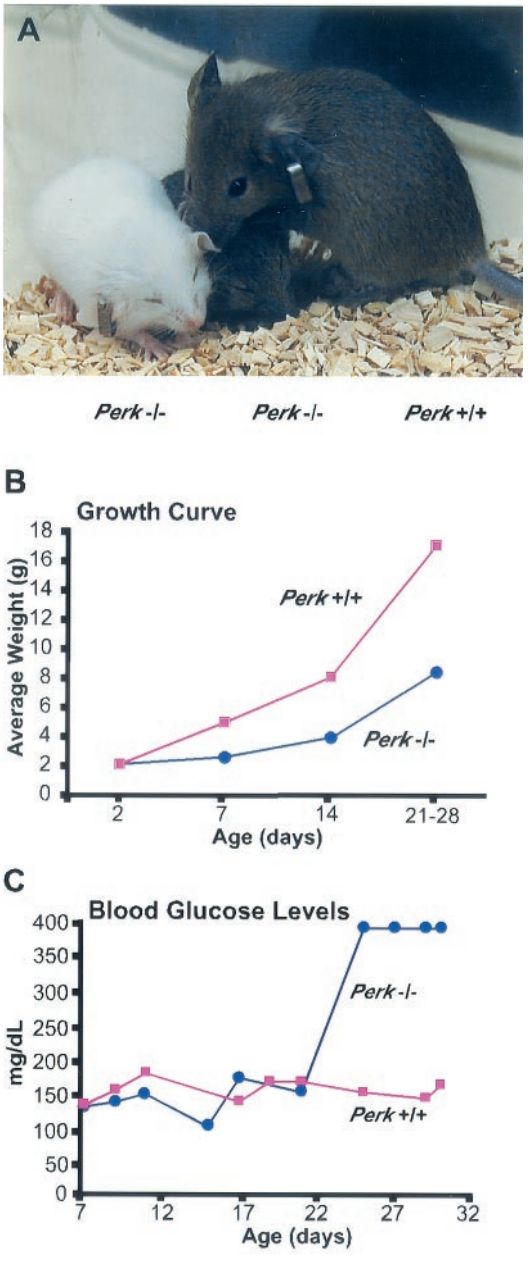

FIG. 3. Postnatal growth retardation and the development of hyperglycemia in *Perk*$^{-/-}$ mice. (A) *Perk*$^{-/-}$ mice (two smaller mice, left) are growth retarded compared to a *Perk*$^{+/+}$ littermate (far right). (B) Growth curve illustrating the average weight for *Perk*$^{+/+}$ and *Perk*$^{-/-}$ littermates plotted against age. (C) Blood glucose levels (in milligrams per deciliter) of *Perk*$^{+/+}$ and *Perk*$^{-/-}$ mice. After postnatal day 22, blood glucose of the *Perk*$^{-/-}$ mice often exceeded the detection capability of the blood glucose monitor.

phometric analysis of the islets indicated a strikingly elevated expression of insulin in a subset of the *Perk*$^{-/-}$ beta cells. A twofold or greater level of insulin content was seen in 21% of the *Perk*$^{-/-}$ beta cells compared to wild-type pancreatic beta cells. Thus, the reduction in the number of beta cells in the *Perk*$^{-/-}$ mice is partially compensated for by overexpression of insulin in the remaining cells. By the end of the sixth week, all of the islets of Langerhans have been lost in some *Perk*$^{-/-}$ mice, and only a few scattered insulin-secreting beta cells and glucagon-secreting alpha cells remain (Fig. 4C, D, and G). The onset of diabetes correlates with the loss of insulin-producing beta cells in the pancreatic islets. Presumably, insulin levels progressively drop below the threshold level needed to maintain normal glycemic control around postnatal day 22. To gain some insight into what this threshold level might be, we measured circulating and pancreatic insulin in prediabetic and di-

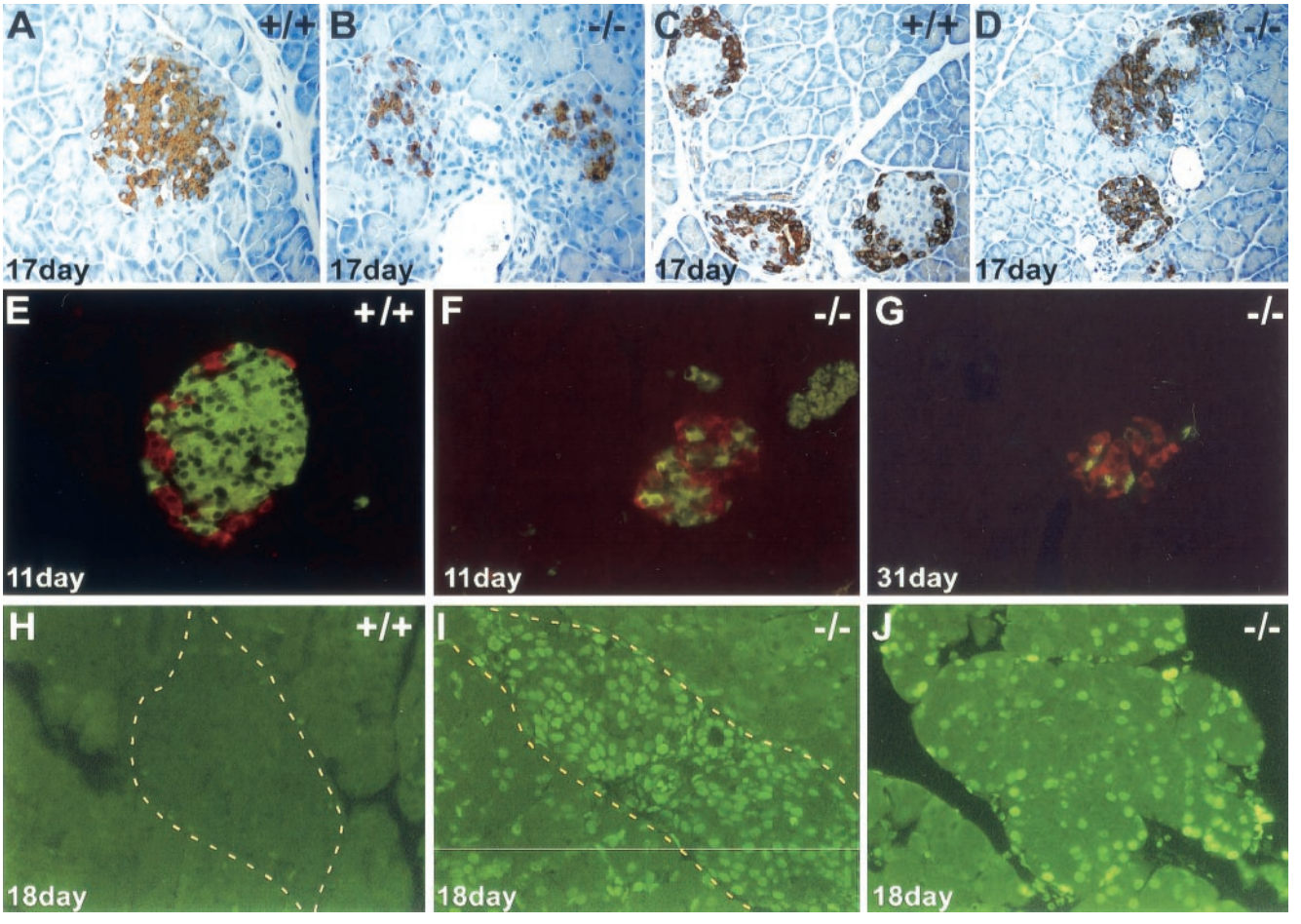

FIG. 4. Apoptotic loss of pancreatic islet of Langerhans and acinar cells in $Perk^{-/-}$ mice. (A and B) Anti-insulin immunostaining of $Perk^{+/+}$ and $Perk^{-/-}$ islets. (C and D) Antiglucagon immunostaining of $Perk^{+/+}$ and $Perk^{-/-}$ islets. Redistribution of the beta cells from the periphery into the central region of the islet has occurred before hyperglycemia has even become apparent. The alpha cells outnumber the beta cells in the mutant islets at this stage, and the entire islet size is drastically reduced. (E to G) Fluorescent double-labeling using Cy2-conjugated donkey anti-guinea pig IgG secondary antibody against guinea pig anti-bovine insulin (green) and Cy3-conjugated donkey anti-rabbit IgG secondary antibody against rabbit antiglucagon (red). (G) Decrease in overall size of the islet and the loss of the alpha and beta cells in a 31-day-old diabetic $Perk^{-/-}$ mouse. (H to J) Apoptosis in an islet (I) and acinar cells (J) detected by TUNEL labeling on 18-day-old $Perk^{-/-}$ mice. Yellow dashed line outlines edges of islets.

abetic $Perk^{-/-}$ mice. Prediabetic *Perk* knockout mice (7 to 11 days old) had 70% of normal pancreatic insulin of wild-type littermates but exhibited serum insulin levels indistinguishable from those in wild-type littermates. In 2-month-old $Perk^{-/-}$ diabetic mice, pancreatic insulin fell to less than 10% of control values, while serum insulin values for $Perk^{-/-}$ were only 5% of normal. The drop in pancreatic and serum insulin was largely reflected in the changes in insulin mRNA. Insulin mRNA in $Perk^{-/-}$ mice was reduced to 65% of normal at postnatal day 13 and to 39% of normal by postnatal day 26. The reduction in insulin mRNA closely mirrored the reduction in the number of insulin-secreting beta cells.

PERK is required for the viability of pancreatic acinar cells and acinar function. The exocrine pancreas appears histologically normal during the first three postnatal weeks, with well-organized acini that are fully loaded with zymogen granules. However, ultrastructural TEM analyses showed that in many acinar cells the ER has become greatly distended and fragmented, allowing the zymogen granules to invade the cytoplasm adjacent to the nucleus (Fig. 5A to D). The abnormal ER in the $Perk^{-/-}$ acinar cells appears to be devoid of protein in the cisternae. In normal acinar cells, the zymogen granules are largely excluded from the periphery of the nucleus due to the dense packing of the ER. By the third and fourth postnatal weeks, the pancreatic acini of some of the mutant mice underwent massive apoptosis (Fig. 4J and 5H) similar to the destruction of the islet beta cells discussed previously. Within each acinus, one or more of the cells had become highly vacuolated and had lost all resemblance to normal acinar cells (Fig. 5H). These cells express a high level of eIF-2α[P], which is apparently generated by one of the other three eIF-2α kinases. The PKR eIF-2α kinase has previously been associated with apoptosis (29, 35) and is likely responsible for this expression. An increase in the number of periacinar fibroblast-like cells, which are adjacent to the acinar cells, was seen in the $Perk^{-/-}$ mice (Fig. 5H). We speculate that this increase in periacinar fibro-

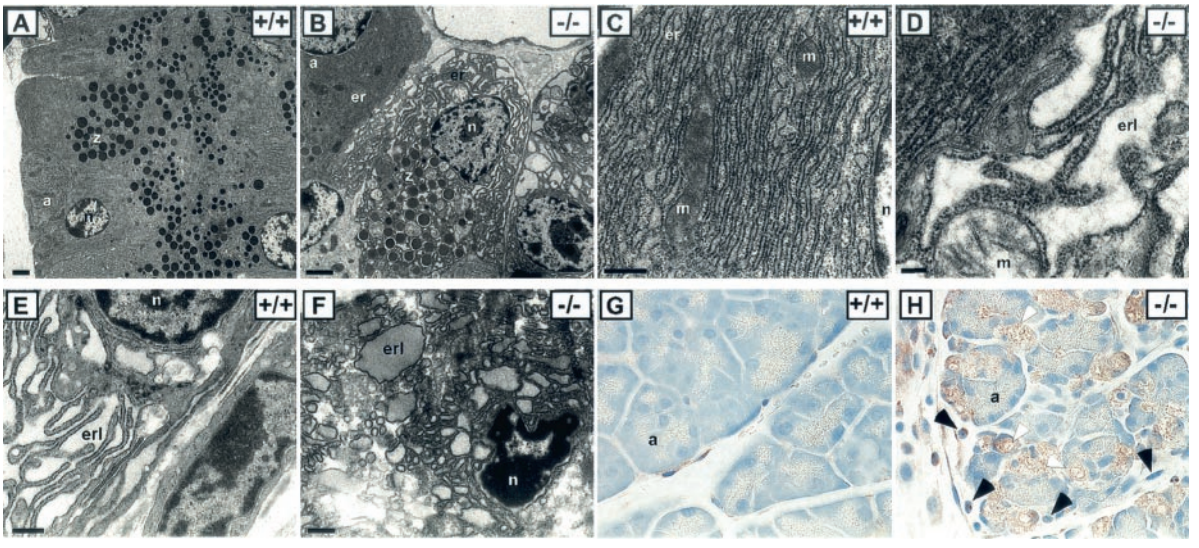

FIG. 5. Cellular and subcellular anomalies in pancreata and bone tissue in *Perk*$^{-/-}$ mice. Pancreatic acinar cells exhibit fragmented and distended ER (er) in *Perk*$^{-/-}$ mice (B and D) compared to that in wild-type mice (A and C). Note the crowding of the zymogen granules (z) around the nucleus in *Perk*$^{-/-}$ acinar cells (B) compared to that in the wild-type cells (A) due to the breakdown of normal ER structure. a, acini; n, nucleus; er, RER; erl, ER lumen; m, mitochondria. Bars: A and B, 2.0 μm; C, D, and E, 0.2 μm. (E) A wild-type osteoblast showing a prototypical RER structure. (F) An osteoblast cell in compact bone tissue of a *Perk*$^{-/-}$ mouse exhibiting highly fragmented and distended ER with densely stained material in the cisternae (erl). (G and H) A large fraction of the pancreatic acinar cells seen in a 32-day-old *Perk*$^{-/-}$ mouse are severely vacuolated and lack zymogen granules (H), compared to a *Perk*$^{+/+}$ pancreas (G). Magnification, ×60. Black arrows in panel H indicate periacinar cells that have proliferated in the *Perk*$^{-/-}$ pancreas, and white arrows indicate vacuolated acinar cells that have apparently succumbed to apoptosis. This tissue section was immunostained (brown) for eIF-2α[P] by using an antisera specific for eIF-2α[P]. The presence of a high level of eIF-2α[P] is highly correlated with abnormally vacuolated acinar cells.

blast-like cells, which is often seen in patients with pancreatitis (4), is a proliferative response to the general apoptosis in the exocrine and endocrine pancreas.

The levels of some of the major digestive enzymes secreted by the acinar cells were measured in pancreatic extracts of prediabetic mice (11 to 12 days old) and diabetic mice (26 to 28 days old) (Table 1). Prediabetic *Perk*$^{-/-}$ mice had significantly lower levels of pancreatic α-amylase, lipase, carboxypeptidase A, DNase, and RNase when compared to wild-type littermates, whereas carboxypeptidase B and trypsinogen levels were similar in the two groups. In contrast, the mRNA levels of these enzymes were not significantly different between the *Perk*$^{-/-}$ mice and their wild-type littermates. The reduction in the level of the five enzymes noted above therefore suggests that the mRNAs which encode them may be translationally repressed or that their posttranslational processing is diminished. Diabetic *Perk*$^{-/-}$ mice (26 to 28 days old) had similarly lower levels of α-amylase (Fig. 2E and Table 1), carboxypeptidase A, and lipase. Differences in the relative amounts of acinar enzymes between the two age groups, especially the increase in pancreatic DNase, may reflect secondary effects of apoptosis that occur in the pancreas of diabetic *Perk*$^{-/-}$ mice.

TABLE 1. Expression of pancreatic hydrolases and insulin in *Perk*$^{-/-}$ mice as a ratio of expression in wild-type mice[a]

Tissue and protein	Relative level of protein	
	Prediabetic[b]	Diabetic[c]
Pancreatic acinar tissue[d]		
α-Amylase	0.48	0.46
Pancreatic lipase	0.25	0.16
Carboxypeptidase A	0.50	0.64
DNase I	0.68	0.91
RNase A	0.42	0.40
Carboxypeptidase B	1.10	0.98
Trypsinogen	1.00	0.75
Insulin[e]		
Total pancreatic insulin	0.70	0.09
Serum insulin	1.01	0.20

[a] Each value represents the average of three or more animals.
[b] Prediabetic mice were 7 to 11 days old.
[c] Diabetic mice were 26 to 28 days old.
[d] Determined by Western immunoblotting and normalized to tubulin or actin.
[e] Determined by ELISA in nanograms of insulin per milliliter of serum, normalized to the wild type.

***Perk*$^{-/-}$ mice exhibit multiple skeletal dysplasias and abnormal expression of collagen I.** PERK is highly expressed in bone tissue at levels comparable to those of the pancreas, suggesting a potential developmental or physiological role of PERK in the skeletal system (Fig. 6A). Consistent with this hypothesis, *Perk*$^{-/-}$ mice exhibit severe spinal curvature (hunchback), splayed hind limbs, and reduced locomotor activity. To determine if these phenotypes are the result of skeletal dysplasias, the total skeletal system was examined after staining whole mice with Alizarin Red and Alcian Blue, which identify mineralized bone and cartilage, respectively. Bone mineralization of the entire skeleton of the *Perk*$^{-/-}$ mice was diminished in bone tissues derived from both intramembranous and endochondral ossification (Fig. 7B, D, and F) compared to wild-type littermates (Fig. 7A, C, and E). The axial skeleton exhibited the most apparent defects (Fig. 7C to H), including compression and asymmetry of the vertebrae (Fig. 7D) and diminished bone density (Fig. 7F). These defects were

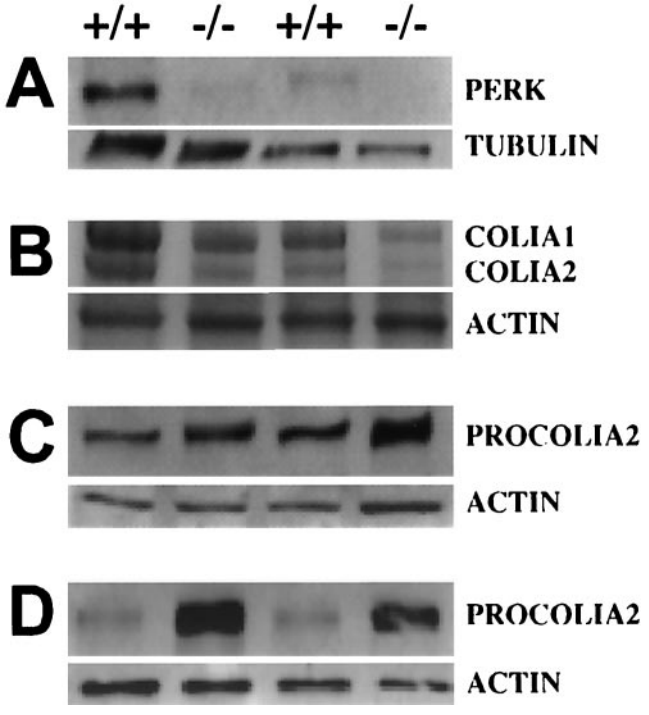

FIG. 6. PERK expression in bone tissue and misregulation of PROCOLIA2 and COLIA2 in *Perk*$^{-/-}$ mice. (A) Immunoblot of PERK in bone tissues (5 μg). Lanes 1 and 2, thoracic vertebrae; lanes 3 and 4, tibial long bones. The faint band present in the *Perk*$^{-/-}$ mutants is due to cross-reactivity with an unrelated protein. (B) COLIA1 and COLIA2 in tibia long bone tissue (lanes 1 and 2) and thoracic vertebrae (lanes 3 and 4) (10 μg). (C) Immunoblot of PROCOLIA2 of tibia long bone tissue (10 μg). (D) Immunoblot of PROCOLIA2 of cultured osteoblasts (10 μg). Quantitative Phosphorimager analysis was performed on these data and on other replicate samples. The large differences in COLIA1, COLIA2, and PROCOLIA2 between *Perk*$^{-/-}$ mice and their wild-type littermates shown here were consistently observed across several litters. PROCOLIA1 is also reduced in *Perk*$^{-/-}$ mice (data not shown), proportionate to the reduction observed in PROCOLIA2.

seen in *Perk*$^{-/-}$ neonates (shown herein) as well as prenatally (results not shown).

Underlying the gross structural anomalies in the *Perk*$^{-/-}$ skeleton, we found defects in compact bone formation in both long bone and flat bone types. Compact bone of long bone collars, the parietal bones of the skull, and the body of the vertebrae exhibited large perforations and discontinuities that compromised their structural integrity (Fig. 7G to M). These perforations and discontinuities allowed the bone marrow to escape the medullary cavity (Fig. 7J). The compact bone of the vertebrae was often greatly reduced in thickness or was even absent in some cases (Fig. 7H). The epiphyseal growth plates of the *Perk*$^{-/-}$ mice appeared to be normal; however, the trabeculae of the spongy bone often exhibited compensatory growth to provide structural integrity in the absence of normal compact bone collar (Fig. 7H). Most of the skeletal defects of the *Perk*$^{-/-}$ mice occurred in the compact bone matrix secreted by osteoblasts. Ultrastructural examination of *Perk*$^{-/-}$ mutants indicated that many, but not all, osteoblasts exhibit highly distended and fragmented ER (Fig. 5F), similar to the ER of mutant pancreatic acinar cells. Some of the mutant osteoblasts exhibited pycnotic nuclei and other signs of apoptosis. The defect in the ER of the *Perk*$^{-/-}$ osteoblasts is similar to that seen in the pancreatic acinar cells with one notable exception: the distended and fragmented ER cisternae of the osteoblasts apparently contain a high protein concentration, whereas the ER cisternae of the acinar cells appear to be protein depleted.

Type I collagen is the major protein constituent of the extracellular matrix comprising compact bone. *Perk*$^{-/-}$ mice exhibited a two- to fourfold reduction in collagen type I α1 and α2 (COLIA1 and COLIA2) (Fig. 6B), as expected from the observed general deficiency of compact bone throughout the skeletal system. However, the corresponding procollagen type I precursor levels were elevated almost twofold in *Perk*$^{-/-}$ bone tissue (Fig. 6C), suggesting that the deficiency in the mature type I collagen is due to a repression of procollagen processing or transport in the ER/Golgi secretory pathway. Primary cultures of osteoblasts isolated from the calvaria of *Perk*$^{-/-}$ mice exhibited an even more pronounced elevation (eightfold) in PROCOLIA2 levels (Fig. 6D) compared to wild-type littermates. We speculate that the electron-dense material seen in the abnormal RER of *Perk*$^{-/-}$ osteoblasts corresponds to unprocessed procollagen and perhaps other bone matrix proteins that accumulate due to a deficiency in ER functions.

DISCUSSION

PERK is required for the function and viability of the pancreas. Approximately one-third of all proteins are synthesized on the RER and are destined for secretion or intracellular functions that require their glycosylation, folding, and targeting in the ER. For highly specialized secretory cells, however, RER-mediated cotranslational synthesis and import dominates the entire regulatory system that controls protein synthesis. Particularly in the endocrine and exocrine pancreas, the regulation of protein synthesis is tied to episodic secretion. Factors that stimulate protein secretion impact not only the translation of secreted proteins but also the expression of genes that underlie the secretory pathway. We show herein that the PERK eIF-2α kinase is highly expressed in the major secretory cells of the endocrine and exocrine pancreas and that the loss of PERK expression ultimately results in catastrophic loss of pancreatic functions by apoptosis. The loss-of-function phenotype of the *Perk*$^{-/-}$ mice may be explained by two alternative hypotheses regarding the normal function of PERK.

Harding and coworkers (13, 14) have proposed that the major function of PERK is to act as a sensor of abnormal stress as part of the UPR. To explain the *Perk*$^{-/-}$ mutant phenotype under this proposal, one must assume that individual secretory cells may periodically experience fluctuating stresses that elicit the UPR in an otherwise normal developmental and physiological context of the whole organism. The progressive apoptosis of the pancreatic secretory cells in *Perk*$^{-/-}$mice over a several-week period is consistent with this hypothesis. We observed the loss of some beta cells as early as the first postnatal week, yet some of the beta cells appeared to synthesize and secrete insulin as late as the fifth postnatal week before succumbing to apoptosis. Harding and coworkers (12) reported similar findings for insulin-secreting beta cells and acinar cells, but they did not report the loss of glucagon-secreting alpha

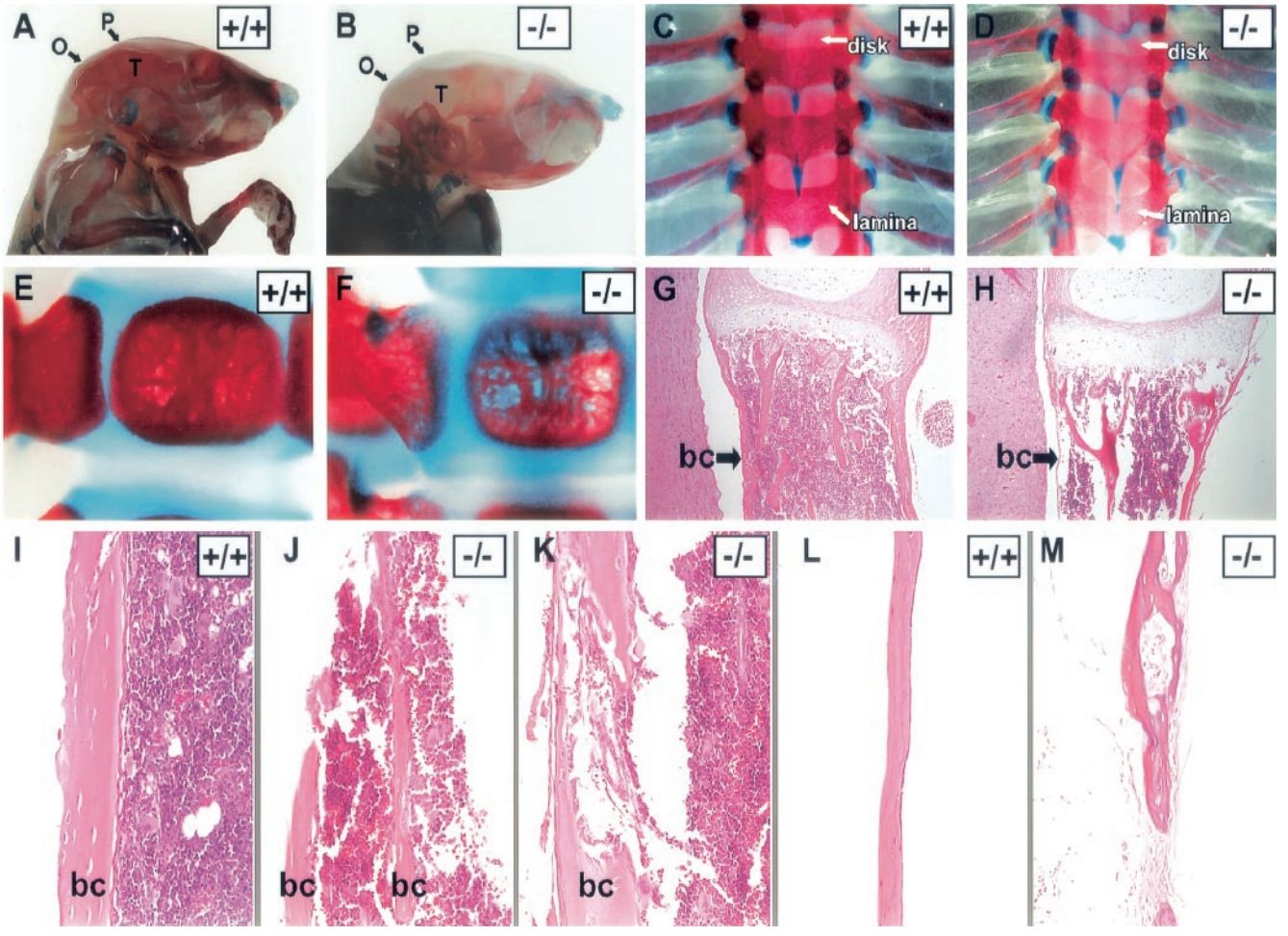

FIG. 7. *Perk*$^{-/-}$ mice display multiple skeletal dysplasias. (A to F) Alizarin Red (mineralized bone) and Alcian Blue (cartilage) skeletal staining of 18-day-old (A to D) and 2-day-old (E and F) mice. The mineralization of the flat bones of the skull (P, parietal; O, occipital; T, temporal) is greatly reduced in the *Perk*$^{-/-}$ mouse (B). (C and D) The *Perk*$^{-/-}$ dorsal thoracic vertebral column shows lack of mineralization across the spine, but especially in the lamina compared to the wild type, as indicated by arrows. Asymmetrical formation and compression of the vertebral column are indicated by arrows pointing to the intervertebral disks. (E and F) Single vertebrae (ventral bodies) of the *Perk*$^{+/+}$ and *Perk*$^{-/-}$ mice (2 days old). Notice the obvious porosity of the vertebrae body in the *Perk*$^{-/-}$ mouse. (G to M) Hematoxylin and eosin staining of *Perk*$^{+/+}$ and *Perk*$^{-/-}$ bones. (G and H) Longitudinal sections of single vertebrae bodies. Arrows point to the three layers of the bone collar (bc), which are extremely thin in the *Perk*$^{-/-}$ vertebrae. (I to K) Tibial sections show the porosity and abnormal formation of the bone collars of long bone. (L and M) The weakness, lack of organization, and porosity of the mutant bones are also apparent in the parietal bones of the skull. Panels B and M are at higher magnification.

cells or the skeletal dysplasias that we show herein. The number of glucagon-secreting alpha cells and acinar cells in the *Perk*$^{-/-}$ mice we describe herein do not appear to decrease until after the third postnatal week. The delay in alpha cell and acinar cell apoptosis may be related to weaning, which occurs shortly before then, or a response to the loss of the insulin-secreting beta cells. The loss of insulin-secreting beta cells via autoimmune destruction is characteristic of type I diabetes mellitus; however, the loss of the other islet cell types seen in the *Perk*$^{-/-}$ mice is not typical of type I diabetic individuals. Moreover, the loss of beta cells in the *Perk*$^{-/-}$ mice is not preceded by the infiltration of mononuclear leukocytes (insulitis) in the islets of Langerhans, as is typical of type I diabetes mellitus.

We propose an alternative hypothesis, that PERK's major function is to negatively regulate global protein synthesis and positively regulate the translation initiation of key mRNAs that underlie normal physiological processes of secretory cells. We have shown that during the fasted state, when protein synthesis in the pancreas is generally repressed, eIF-2α is heavily phosphorylated by PERK. Protein synthesis in the pancreas is induced by glucose within 30 min (11), and we showed that dephosphorylation of eIF-2α begins shortly before the induction of protein synthesis, suggesting that the repression of protein synthesis in the fasted state is caused by phosphorylation of eIF-2α by PERK. We propose that when secretory cells reach their protein storage and folding capacity in the ER, PERK is activated by its disassociation from BiP/GRP78 and the reduction in Ca^{2+}, which normally occurs under these conditions (8, 37). This regulatory mechanism allows secretory cells to maximize, without exceeding, the storage capacity of proteins. This form of regulation is particularly relevant to

secretory cells that respond to episodic stimuli. We propose that some of the abnormalities observed in the *Perk*$^{-/-}$ mice are due to uncontrolled protein synthesis that exceeds the storage capacity of secretory cells and subsequently leads to the induction of apoptosis. The overexpression of insulin in some of the islet beta cells of *Perk*$^{-/-}$ mice, followed by apoptosis, is consistent with this hypothesis. Harding and coworkers (12) also reported an increase in insulin synthesis in isolated islets of Langerhans from *Perk*$^{-/-}$ mutant mice.

In addition to negatively regulating global protein synthesis, phosphorylation of eIF-2α by PERK is likely to activate the translation of specific mRNAs. We show herein that the level of several major digestive enzymes synthesized by the exocrine pancreas are down-regulated in *Perk*$^{-/-}$ neonatal mice prior to the onset of apoptosis, although the levels of the mRNAs which encode them remain high. These findings are consistent with PERK selectively activating the translation of these mRNAs in normal mice. Translation of these specific mRNAs may be activated at the initiation stage as a function of specific mRNA sequence elements analogous to the selective translational derepression of yeast GCN4 mediated by the GCN2 eIF-2α kinase. Preliminary experiments indicate that a number of genes encoding proteins that participate in secretory processes are repressed in the pancreata of *Perk*$^{-/-}$ neonatal mice (unpublished data) prior to the onset of apoptosis. We are currently investigating the expression of these genes in the context of PERK regulatory functions.

PERK is essential for bone development. Phosphorylation of eIF-2α has been observed in a large number of physiological and developmental contexts, leading to a recurrent speculation that the eIF-2α kinases may have important roles in development. Yet, mouse knockout mutations of the other three eIF-2α kinases (PKR, HRI, and GCN2) are not associated with overt developmental defects. We show herein, however, that PERK is required for prenatal and postnatal bone development. At birth, *Perk*$^{-/-}$ mutants display osteoporosis and deficient mineralization throughout the skeletal system. Compact bone either is greatly reduced or exhibits perforations and discontinuities. These defects are similar to those seen in human patients with osteogenesis imperfecta, a disease associated with reduced or defective collagen synthesis (41). Compact bone is composed of extracellular bone matrix, of which type I collagen is the major protein. Procollagen type I α1 and α2 chains are cotranslationally imported into the ER, where they become posttranslationally modified and form procollagen triple helices of two α1 chains and one α2 chain. Procollagen type I triple helix is secreted, whereupon it is proteolytically processed to form mature type I collagen. Procollagen type I accumulates to abnormally high levels in bone tissue and primary cultures of osteoblasts from *Perk*$^{-/-}$ mice, whereas mature type I collagen is deficient. In addition, osteoblasts exhibit fragmented and distended ER containing electron-dense material. We speculate that in the absence of PERK, the secretory pathway in osteoblasts is compromised and cannot efficiently process and secrete procollagen, thus leading to the accumulation of procollagen and distention of the ER cisternae.

The pancreatic and skeletal deformities of *Perk*$^{-/-}$ mice are similar to those of human WRS. Although numerous pleiotropic effects have been reported in humans with diabetes mellitus, dwarfism and skeletal dysplasias are not typically associated with this disease. However, the Wolcott-Rallison syndrome (WRS), a rare genetic disease, is characterized by the cooccurrence of an early onset of insulin-dependent diabetes, dwarfism, and skeletal dysplasias (36) very similar to the defects seen in the *Perk*$^{-/-}$ mice. Based upon only two families, WRS was mapped to the human *Perk* gene (7). Single nucleotide differences in the *Perk* gene of the WRS individuals were interpreted as putative loss-of-function mutations; however, molecular evidence of the absence of PERK was lacking. Our finding that a deletion of critical domains of PERK results in a WRS phenotype in mice provides conclusive evidence that the loss of PERK function results in this complex mutant phenotype. The function of PERK in bone growth and development may be cell-autonomous to bone tissue. Alternatively, PERK may be regulating the synthesis of growth hormone or other growth factors produced by endocrine organs that are known to regulate bone development. In WRS patients, severe diabetes mellitus typically develops within the first six postnatal weeks, but growth retardation and skeletal dysplasias have not been detected until several months after birth. *Perk*$^{-/-}$ mice develop diabetes mellitus a few weeks earlier than humans and growth retardation is evident at the end of the first postnatal week; thus, the order of the development of these phenotypes in mice and humans is reversed. The difference in the order of occurrence of these anomalies is likely because mice normally grow much more quickly during the first few postnatal weeks than humans. We speculate that the skeletal dysplasias associated with the loss of PERK function in humans are not evident to cursory medical examination of newborn babies and that noninvasive bone-density tomography of suspected WRS babies would reveal infantile osteoporosis.

The PERK eIF-2α kinase is thought to have a single substrate, the Ser51 residue of eIF-2α, and therefore we propose that the complex array of defects observed in the *Perk*$^{-/-}$ mutants is due to misregulation of the eIF-2–GTP–Met-tRNAi ternary complex, an essential component of translation initiation. However, the PKR eIF-2α kinase has been shown to have at least one other substrate (21) in addition to Ser51 eIF-2α, raising the possibility that PERK may have other substrates as well. To address the biochemical defects underlying the loss of eIF-2α kinase functions, Scheuner and coworkers (31) have generated a Ser51Ala eIF-2α knock-in mutation in mice that ablates phosphorylation at this site. These mice die within 18 h after birth due to hypoglycemia associated with defects in gluconeogenesis. In addition, these mice exhibit reduced insulin levels, apparently due to a reduction in the number of insulin-secreting beta cells. The loss of insulin-secreting beta cells in the Ser51Ala eIF-2α mutant mice is similar to that observed in *Perk* mutant mice, although the loss of beta cells is accelerated in the former. *Perk*$^{-/-}$ mice, however, are euglycemic for the first 3 weeks after birth before becoming severely hyperglycemic. Two other eIF-2α kinases, GCN2 and PKR, are known to be expressed in both liver and pancreas (22, 33) and may contribute to glucose homeostasis. *Gcn2* (unpublished data) and *Pkr* (1, 42) knockout mice do not exhibit overt defects in glucose homeostasis but may collectively regulate pancreatic and liver functions in concert with PERK.

ACKNOWLEDGMENTS

We thank Lillian B. Nanney and Kelly Parman of the Mouse Pathology and Immunohistochemistry Core Lab at Vanderbilt University Medical Center for their help with the processing and immunostaining of mouse tissues. We gratefully acknowledge Mark Magnuson of the Transgenic Mouse/Embryonic Stem Cell Shared Resource at Vanderbilt University Medical Center for his assistance with the design of the targeted *Perk* knockout, and we thank Cathleen Pettepher for her help in generating the *Perk* knockout mice. Our thanks also go to the staff of the Electron Microscopy Facility at the Pennsylvania State University for their technical assistance with transmission electron microscopy and immunohistochemistry, to Jeffery O'Neil for his help with monitoring mouse growth and blood glucose levels, and to Donna Brantlinger Black for her help with preparation of the manuscript. Finally, we thank Ronald Wek for providing PERK cDNA clones, DNA sequence information, anti-PERK (hPEK) antisera, and valuable discussions throughout this work.

This work was supported by the Culpeper Foundation, the Vanderbilt Clinical Nutrition Research Unit, The Pennsylvania State University, and National Institutes of Health grant GM56957 (to D.R.C.).

REFERENCES

1. **Abraham, N., D. F. Stojdl, P. I. Duncan, N. Methot, T. Ishii, M. Dube, B. C. Vanderhyden, H. L. Atkins, D. A. Gray, M. W. McBurney, A. E. Koromilas, E. G. Brown, N. Sonenberg, and J. C. Bell.** 1999. Characterization of transgenic mice with targeted disruption of the catalytic domain of the double-stranded RNA-dependent protein kinase, PKR. J. Biol. Chem. **274:**5953–5962.
2. **Berlanga, J. J., J. Santoyo, and C. De Haro.** 1999. Characterization of a mammalian homolog of the GCN2 eukaryotic initiation factor 2α kinase. Eur. J. Biochem. **265:**754–762.
3. **Bertolotti, A., Y. Zhang, L. M. Hendershot, H. P. Harding, and D. Ron.** 2000. Dynamic interaction of BiP and ER stress transducers in the unfolded-protein response. Nat. Cell Biol. **2:**326–332.
4. **Casini, A., A. Galli, P. Pignalosa, L. Frulloni, C. Grappone, S. Milani, P. Pederzoli, G. Cavallini, and C. Surrenti.** 2000. Collagen type I synthesized by pancreatic periacinar stellate cells (PSC) co-localizes with lipid peroxidation-derived aldehydes in chronic alcoholic pancreatitis. J. Pathol. **192:**81–89.
5. **Chen, J. J., and I. M. London.** 1995. Regulation of protein synthesis by heme-regulated eIF-2 alpha kinase. Trends Biochem. Sci. **20:**105–108.
6. **Clemens, M. J.** 1996. Protein kinases that phosphorylate eIF-2 and eIF-2B, and their role in eukaryotic cell translational control, p. 139–172. *In* J. W. B. Hershey, M. B. Mathews, and N. Sonenberg (ed.), Translational control. Cold Spring Harbor Laboratory, Plainview, N.Y.
7. **Delepine, M., M. Nicolino, T. Barrett, M. Golamaully, G. M. Lathrop, and C. Julier.** 2000. EIF-2AK3, encoding translation initiation factor 2-alpha kinase 3, is mutated in patients with Wolcott-Rallison syndrome. Nat. Genet. **25:**406–409.
8. **Easom, R. A.** 2000. Beta-granule transport and exocytosis. Semin. Cell Dev. Biol. **11:**253–266.
9. **Ecarot-Charrier, B., F. H. Glorieux, M. van der Rest, and G. Pereira.** 1983. Osteoblasts isolated from mouse calvaria initiate matrix mineralization in culture. J. Cell Biol. **96:**639–643.
10. **Gilmore, R., G. Blobel, and P. Walter.** 1982. Protein translocation across the endoplasmic reticulum. I. Detection in the microsomal membrane of a receptor for the signal recognition particle. J. Cell Biol. **95:**463–469.
11. **Goodge, K. A., and J. C. Hutton.** 2000. Translational regulation of proinsulin biosynthesis and proinsulin conversion in the pancreatic beta-cell. Semin. Cell Dev. Biol. **11:**235–242.
12. **Harding, H. P., H. Zeng, Y. Zhang, R. Jungries, P. Chung, H. Plesken, D. D. Sabatini, and D. Ron.** 2001. Diabetes mellitus and exocrine pancreatic dysfunction in perk-/- mice reveals a role for translational control in secretory cell survival. Mol. Cell **7:**1153–1163.
13. **Harding, H. P., Y. Zhang, A. Bertolotti, H. Zeng, and D. Ron.** 2000. Perk is essential for translational regulation and cell survival during the unfolded protein response. Mol. Cell **5:**897–904.
14. **Harding, H. P., Y. Zhang, and D. Ron.** 1999. Protein translation and folding are coupled by an endoplasmic-reticulum-resident kinase. Nature **397:**271–274.
15. **Hershey, J. W.** 1991. Translational control in mammalian cells. Annu. Rev. Biochem. **60:**717–755.
16. **Hinnebusch, A. G.** 1994. The eIF-2 alpha kinases: regulators of protein synthesis in starvation and stress. Semin. Cell Biol. **5:**417–426.
17. **Hinnebusch, A. G.** 1996. Translational control of *GCN4*: gene-specific regulation by phosphorylation of eIF-2, p. 199–244. *In* J. W. B. Hershey, M. B. Mathews, and N. Sonenberg (ed.), Translational control. Cold Spring Harbor Laboratory, Plainview, N.Y.
18. **Hinnebusch, A. G.** 1997. Translational regulation of yeast GCN4. A window on factors that control initiator-tRNA binding to the ribosome. J. Biol. Chem. **272:**21661–21664.
19. **Itoh, N., T. Sei, K. Nose, and H. Okamoto.** 1978. Glucose stimulation of the proinsulin synthesis in isolated pancreatic islets without increasing amount of proinsulin mRNA. FEBS Lett. **93:**343–347.
20. **Kaufman, R. J.** 1999. Stress signaling from the lumen of the endoplasmic reticulum: coordination of gene transcriptional and translational controls. Genes Dev. **13:**1211–1233.
21. **Kumar, A., J. Haque, J. Lacoste, J. Hiscott, and B. R. Williams.** 1994. Double-stranded RNA-dependent protein kinase activates transcription factor NF-κB by phosphorylating I κB. Proc. Natl. Acad. Sci. USA **91:**6288–6292.
22. **Ladiges, W., J. Morton, C. Blakely, and M. Gale.** 2000. Tissue specific expression of PKR protein kinase in aging B6D2F1 mice. Mech. Ageing Dev. **114:**123–132.
23. **Lakso, M., J. G. Pichel, J. R. Gorman, B. Sauer, Y. Okamoto, E. Lee, F. W. Alt, and H. Westphal.** 1996. Efficient in vivo manipulation of mouse genomic sequences at the zygote stage. Proc. Natl. Acad. Sci. USA **93:**5860–5865.
24. **Morris, G. E., and A. Korner.** 1970. The effect of glucose on insulin biosynthesis by isolated islets of Langerhans of the rat. Biochim. Biophys. Acta **208:**404–413.
25. **Nicchitta, C., G. Migliaccio, and G. Blobel.** 1991. Reconstitution of secretory protein translocation from detergent-solubilized rough microsomes. Methods Cell Biol. **34:**263–285.
26. **Perkins, P. S., J. H. Park, and S. J. Pandol.** 1997. The role of calcium in the regulation of protein synthesis in the exocrine pancreas. Pancreas **14:**133–141.
27. **Permutt, M. A.** 1974. Effect of glucose on initiation and elongation rates in isolated rat pancreatic islets. J. Biol. Chem. **249:**2738–2742.
28. **Rastogi, G. K., J. Letarte, and T. R. Fraser.** 1970. Immunoreactive insulin content of 203 pancreases from fetuses of healthy mothers. Diabetologia **6:**445–446.
29. **Saelens, X., M. Kalai, and P. Vandenabeele.** 2001. Translation inhibition in apoptosis: caspase-dependent PKR activation and eIF-2-α phosphorylation. J. Biol. Chem. **276:**41620–41628.
30. **Scheele, G. A.** 1993. Regulation of pancreatic gene expression in response to hormones and nutritional substrates, p. 103–120. *In* V. L. W. Go (ed.), The pancreas: biology, pathobiology, and disease. Raven Press, New York, N.Y.
31. **Scheuner, D., B. Song, D. McEwen, L. Chuan, R. Laybutt, P. Gillespie, T. Saunders, S. Bonner-Weir, and R. J. Kaufman.** 2001. Translational control is required for the unfolded protein response and in vivo glucose homeostasis. Mol. Cell **7:**1165–1176.
32. **Shi, Y., K. M. Vattem, R. Sood, J. An, J. Liang, L. Stramm, and R. C. Wek.** 1998. Identification and characterization of pancreatic eukaryotic initiation factor 2α subunit kinase, PEK, involved in translational control. Mol. Cell. Biol. **18:**7499–7509.
33. **Sood, R., A. C. Porter, D. A. Olsen, D. R. Cavener, and R. C. Wek.** 2000. A mammalian homologue of GCN2 protein kinase important for translational control by phosphorylation of eukaryotic initiation factor-2α. Genetics **154:**787–801.
34. **Sood, R., A. C. Porter, K. Ma, L. A. Quilliam, and R. C. Wek.** 2000. Pancreatic eukaryotic initiation factor-2α kinase (PEK) homologues in humans, *Drosophila melanogaster* and *Caenorhabditis elegans* that mediate translational control in response to endoplasmic reticulum stress. Biochem. J. **346**(Pt. 2)**:**281–293.
35. **Srivastava, S. P., K. U. Kumar, and R. J. Kaufman.** 1998. Phosphorylation of eukaryotic translation initiation factor 2 mediates apoptosis in response to activation of the double-stranded RNA-dependent protein kinase. J. Biol. Chem. **273:**2416–2423.
36. **Stoβ, H., H. J. Pesch, B. Pontz, A. Otten, and J. Spranger.** 1982. Wolcott-Rallison syndrome: diabetes mellitus and spondyloepiphyseal dysplasia. Eur. J. Pediatr. **138:**120–129.
37. **Tengholm, A., B. Hellman, and E. Gylfe.** 1999. Glucose regulation of free Ca^{2+} in the endoplasmic reticulum of mouse pancreatic beta cells. J. Biol. Chem. **274:**36883–36890.
38. **Walter, P., and V. R. Lingappa.** 1986. Mechanism of protein translocation across the endoplasmic reticulum membrane. Annu. Rev. Cell Biol. **2:**499–516.
39. **Wek, R. C.** 1994. eIF-2 kinases: regulators of general and gene-specific translation initiation. Trends Biochem. Sci. **19:**491–496.
40. **Welsh, M., N. Scherberg, R. Gilmore, and D. F. Steiner.** 1986. Translational control of insulin biosynthesis. Evidence for regulation of elongation, initiation and signal-recognition-particle-mediated translational arrest by glucose. Biochem. J. **235:**459–467.
41. **Willing, M. C., D. H. Cohn, B. Starman, K. A. Holbrook, C. R. Greenberg, and P. H. Byers.** 1988. Heterozygosity for a large deletion in the alpha 2(I) collagen gene has a dramatic effect on type I collagen secretion and produces perinatal lethal osteogenesis imperfecta. J. Biol. Chem. **263:**8398–8404.
42. **Yang, Y. L., L. F. Reis, J. Pavlovic, A. Aguzzi, R. Schafer, A. Kumar, B. R. Williams, M. Aguet, and C. Weissmann.** 1995. Deficient signaling in mice devoid of double-stranded RNA-dependent protein kinase. EMBO J. **14:**6095–6106.